

Formation of Self-Assembled Monolayers of Semifluorinated and Hydrocarbon Chlorosilane Precursors on Silica Surfaces from Liquid Carbon Dioxide

Kirill Efimenko,[†] Brian Novick,[†] Ruben G. Carbonell,[†]
Joseph M. DeSimone,^{†,‡} and Jan Genzer^{*,†}

Department of Chemical Engineering, North Carolina State University,
Raleigh, North Carolina 27695-7905, and Department of Chemistry, University of
North Carolina at Chapel Hill, Chapel Hill, North Carolina 27599-3290

Received December 17, 2001. In Final Form: May 13, 2002

We report on the formation and properties of self-assembled monolayers (SAMs) prepared by depositing semifluorinated and hydrocarbon trichlorosilane precursors, $F(CF_2)_8(CH_2)_2SiCl_3$ (F8H2) and $H(CH_2)_{18}SiCl_3$ (H18), respectively, from vapor, organic solvent, and liquid CO_2 (l- CO_2). Contact angle measurements of the SAM deposition kinetics reveal that regardless of the molecule type, the deposition rates from l- CO_2 exceed those from vapor or organic solvents by several orders of magnitude. We derive two different transport models describing the formation of SAMs. We show that while the diffusion-limited model is not capable of describing the experimental data, the adsorption-limited model captures the major features of the adsorption kinetics quite well. We apply the results of the adsorption-limited model to conclude that the observed behavior is a consequence of (i) a relatively high bulk concentration (l- CO_2 vs vapor) and (ii) higher solution diffusivity (l- CO_2 vs organic solvent) of the silanes in l- CO_2 . Near-edge X-ray absorption fine structure (NEXAFS) is used to monitor the orientation of the F8H2 and H18 molecules in their corresponding SAMs as a function of time. Our NEXAFS data show that the F8H2 molecules adsorb initially from l- CO_2 without any molecular order in the monolayer. As more F8H2 molecules partition at the silicon oxide surface, they start to organize and orient. A complete monolayer order is achieved after ≈ 30 min exposure to F8H2/l- CO_2 solutions. The deposition kinetics and molecular behavior of the H18 moieties in the SAMs are found to be different, however. After a brief exposure (< 2 s) of the silica substrate to the H18/l- CO_2 solution, the molecules adsorb and form an organized monolayer. Similar to the case of the semifluorinated species, the order in the H18 SAM increases with increasing time and saturates after ≈ 5 min exposure to H18/l- CO_2 solution. We attribute the difference in the orientation kinetics to the different solubilities of F8H2 and H18 in l- CO_2 .

Introduction

Thin polymeric films have long been recognized as important for tailoring the characteristics of materials surfaces.¹ With recent advances in nanotechnology, calling for decreases in the feature sizes of nanodevices and microelectronic components to the nanometer scale, the need for a new class of interfacial modifiers with sizes comparable to the dimension of a single molecule becomes even more eminent. Such surfaces with nanometer thick and structurally well-defined surface modifiers can be prepared by depositing self-assembled monolayers (SAMs) or Langmuir–Blodgett films.² Some of the most commonly used molecules forming SAMs are those bearing either (i) a mercapto group that can be terminally attached to gold (or other noble metal) surfaces or (ii) a chloro- or alkoxy-silane moiety capable of reacting with a hydroxy terminus on the surface. The application of the latter family of compounds is particularly useful for modifying the surfaces of silicon and other semiconductor surfaces that are covered with a thin (\approx several nanometers) native oxide layer. These molecules consisting of a hydrocarbon (R^* -) chain bonded to a functionalized Si

group exist either in the form of chlorosilanes, for example, mono ($R^*-SiClR_2$), di- (R^*-SiCl_2R), or tri-chlorosilanes (R^*-SiCl_3), or alkoxy-silanes, for example, mono- ($R^*-SiCl(OR)_2$), di- (R^*-SiCl_2OR), or tri-alkoxy-silanes ($R^*-Si(OR)_3$), where R is an alkyl. SAMs based on these compounds can be utilized to tailor surface properties of materials, making them suitable for biocompatibility, biosensors, the reduction of corrosion rates, pattern creation (lithographic processes), friction reduction (useful in microelectromechanical systems, MEMS, technology), foul resistance, modification of membrane properties, and changes in hydrophobicity.³

Current techniques practiced to apply silane-based SAMs on materials surfaces involve either vapor- or liquid-phase depositions. However, there are several challenges that must be resolved before SAMs can become widely used in technological processes. First, the environmental impact of both vapor and liquid deposition processes is of considerable importance and must be minimized. Problems also exist for liquid deposition techniques since they use large quantities of organic solvents. Although deposition from the vapor phase does not require large quantities of potentially harmful solvents, it can be environmentally dangerous because it requires volatile precursors.⁴ The second major problem with integrating SAMs into industrial processes is associated with the rather lengthy

* Corresponding author. E-mail: jan_genzer@ncsu.edu. Phone: +1-919-515-2069.

[†] North Carolina State University.

[‡] University of North Carolina at Chapel Hill.

(1) Koberstein, J. T. (Ed.) Polymer surfaces and interfaces. *MRS Bull.* **1996**, 21 (1), 16–53 (a collection of articles).

(2) Ulman, A., *An Introduction to Ultrathin Organic Films from Langmuir–Blodgett to Self-Assembly*; Academic Press: New York, 1991.

(3) Swalen, J. D., et al. *Langmuir* **1987**, 3, 932. Allara, D. L. *Biosens. Bioelectron.* **1995**, 10, 771. Ulman, A. *Chem. Rev.* **1996**, 96, 1533.

(4) The release of volatile organic compounds (VOC), including vapor-phase precursors and organic solvents, is controlled by the U.S. Environmental Protection Agency.

deposition times.⁵ Production of the SAM requires that the precursors contact the substrate for times ranging from many minutes to as long as several days. This is not viable for manufacturing goods. Other problems include short pot life for solutions and expensive equipment.

Compressed carbon dioxide (CO₂), either in the liquid or supercritical state ($T_c = 31\text{ }^\circ\text{C}$ and $P_c = 1070\text{ psi}$, where T_c and P_c are the critical temperature and critical pressure, respectively), is a benign solvent that should be considered as a viable substitute for current SAM deposition media. In addition to the obvious environmental benefits, CO₂ has many possible technological advantages. The low viscosity of CO₂ should decrease the amount of time necessary for absorption and reaction of the SAM precursor with the surface. Low molecular weight SAM precursors typically have diffusion coefficients in supercritical CO₂ (sc-CO₂) and liquid CO₂ (l-CO₂) of $\approx 10^{-8}\text{ m}^2/\text{s}$, which is about an order of magnitude larger than the diffusion coefficients of the same liquids in typical organic solvents and water.⁶ The compressible nature of CO₂ is another added benefit because it can be used to tune solvent properties. For example, the density of l-CO₂ can be varied from 928 to 466 kg/m³ by raising the temperature from 0 to 31.06 °C (T_c). Similarly, the density of sc-CO₂ can be varied by adjusting the temperature and pressure. This "tunability" is well recognized in the literature and is one of the main reasons why investigators have looked at using CO₂ for processes such as coatings, extractions, polymerizations, particle formation, and foaming.⁷ Last, carbon dioxide has an advantage over typical organic solvents because separation and recovery from many coating compounds can be accomplished by decreasing the pressure.

Several research groups have begun to recognize the benefits of CO₂ and investigate the deposition of SAMs from carbon dioxide. Tripp et al. have used infrared spectroscopy to show that hexamethyldisilazane and octadecyltrichlorosilane can be used to create SAMs on fumed silica.⁸ The amine-functionalized silane experiments do not require water and are therefore performed using surfaces dried with carbon dioxide. Although SAMs are formed, the authors point out that the formation of ammonium carbamate can "block or poison a portion of the Si-OH sites for reaction." Tripp et al. also show that chlorosilanes form SAMs on silica without any significant hydrolysis, which is in contrast to normal solvents. Cao et al. have studied the deposition of SAMs onto silica-covered substrates in l-CO₂ and sc-CO₂ using monochloro-, dichloro-, trichloro-, and dimethylamino silanes.⁹ Reaction kinetics show that amino silanes such as dimethylamino silanes react with silicon surfaces after 3 min. Interestingly, after 10 min there is a slight decrease in contact angle that authors attribute to an increase in packing density and a decrease in rotational ability. Cao and co-workers also show that chlorosilanes react with pretreated silica surfaces after 24 h. Comparison with SAMs formed from toluene shows that monochlorosilane-derived com-

pounds have smaller contact angles when formed from CO₂ but dialkyldichlorosilanes and alkyltrichlorosilanes exhibit similar or higher contact angles when formed from CO₂. Furthermore, the layers formed from the dialkyldichlorosilanes and alkyltrichlorosilanes are oligomeric and not a monolayer. Weinstein et al. have formed monolayers on gold substrates using *n*-alkanethiolate in supercritical CO₂.¹⁰ The SAMs deposited in sc-CO₂ formed as quickly as 5 min and had higher crystallinity and packing density than those formed from organic solvents.

Despite recent progress in CO₂-based deposition processes, many questions relevant to the formation and properties of SAMs deposited from CO₂ remain to be answered. First, carbon dioxide has a large quadrupole moment, but no dipole moment, as well as a moderate polarizability.¹¹ This may lead to differences in the way various molecules behave in CO₂ compared to organic solvents. For example, only fluorinated and silicene compounds are known to have high solubility in carbon dioxide. Recently, it has also been shown that fluorinated species may have specific interactions with carbon dioxide.¹¹ Although it has been recognized that these CO₂-specific properties may significantly affect the kinetic and thermodynamic factors governing the deposition of SAMs from CO₂, there is a lack of research in this area. For example, limited information exists on how the presence of fluorine in SAM precursors affects the kinetics of the deposition process. The orientation of molecules absorbed to the surface has also not been studied extensively. Our current knowledge of the surface properties of CO₂-deposited SAMs comes mainly from contact angle measurements and experiments using X-ray photoelectron spectroscopy (XPS or ESCA). While useful in providing information about the wettability and to some extent also about the structural characteristics of the SAM surfaces, the contact angle measurements offer only an indirect measurement of the surface properties of SAMs. The contact angle of a fluid is known to depend on many factors including surface roughness, surface energy, and even the rate of movement at the contact line.¹² In addition, it mandates placing liquid onto the film surface, which can cause rearrangement of surface molecules, chemical reaction, or swelling. More chemical information about the structure of the monolayer can in principle be obtained from XPS measurements. However, no additional knowledge about the molecular order of the molecules in the SAMs can be gained from XPS. Hence, a complete understanding of the surface requires supplemental measurements utilizing other surface probes.

The goal of this work is 2-fold. First, we study the kinetics of SAM formation from vapor, organic solvent, and l-CO₂. As detailed later in the paper, we find that regardless of the molecule the deposition rates from l-CO₂ far exceed those from vapor and from organic solvent. We note that similar conclusions have also been reached in a very recent work by Cao and co-workers.⁹ However, in contrast to the results reported in ref 9 we use saturated liquid CO₂ in our experiments. Depositing SAMs from l-CO₂ in which a gas/liquid interface is present has several advantages. It allows our precursor solution to be completely mixed before contact with the substrate and not to be diluted as it is added to the SAM coating chamber. In this way, deposition data at very short contact times (\approx seconds), not reported in ref 9, can be reached. Second,

(5) Van Alsten, J. G. *Langmuir* **1999**, *15*, 7605.

(6) Matthews, M. A., et al. *J. Supercrit. Fluids* **2000**, *18*, 141. Lu, X., et al. *Fluid Phase Equilib.* **2000**, *172*, 279.

(7) Tepper, G.; Levit, N. *Ind. Eng. Chem. Res.* **2000**, *39*, 4445. Webb, P. B., et al. *Pure Appl. Chem.* **2000**, *72*, 1347. Tipnis, S. J. *Pop. Plast. Packag.* **2001**, *46*, 77. Matson, D. W., et al. *J. Mater. Sci.* **1987**, *22*, 1919. DeBenedetti, P. G., et al. *Fluid Phase Equilib.* **1993**, *82*, 311. DeSimone, J. M., et al., *Plast. Eng.* **1997**, *53*, 37. Carbonell, R. G., et al. Coatings from liquid and supercritical carbon dioxide. 217th ACS National Meeting, 1999. Royer, J. R., et al. *J. Polym. Sci., Part B: Polym. Phys.* **2000**, *38*, 3168.

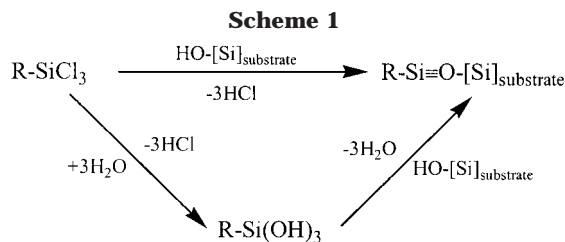
(8) Tripp, C. P.; Combes, J. R. *Langmuir* **1998**, *14*, 7348. Combes, J. R.; White, L. D.; Tripp, C. P. *Langmuir* **1999**, *15*, 7870.

(9) Cao, C.; Fadeev, A. Y.; McCarthy, T. J. *Langmuir* **2001**, *17*, 757.

(10) Weinstein, R. D.; Yan, D.; Jennings, G. K. *Ind. Eng. Chem. Res.* **2000**, *40*, 2046.

(11) Samulski, E. T., et al. *J. Phys. Chem.* **1998**, *102*, 1775.

(12) Neumann, A. W.; Kwok, D. Y. *Adv. Colloid Interface Sci.* **1999**, *81*, 167.



using saturated l-CO_2 allowed for the removal of the entire precursor fluid after formation of the SAM while at constant pressure. This combined with a subsequent rinse with pure CO_2 removes any physisorbed species. In contrast to the Cao et al. experiments, we did not dry or prewet silica substrates. Instead, water for the grafting reaction was supplied by combining high-purity carbon dioxide with moderately humid air during pressurization.

The second goal of our work was to investigate the kinetics of SAM formation for both CO_2 -solvophobic (hydrocarbon) and CO_2 -solvophilic (semifluorinated) molecules. We used ellipsometry to monitor the thickness of the SAMs and near-edge absorption fine structure (NEXAFS) to probe the orientation of the molecules in the SAMs as a function of the deposition time. Thus, by combining the contact angle, ellipsometry, and NEXAFS data we were able to obtain a complete picture of the molecular organization of the hydrocarbon and semifluorinated molecules in their respective SAMs. The NEXAFS measurements were particularly important because they helped us to explain qualitatively why the hydrocarbon-based SAMs form faster than their semifluorinated counterparts.

Experimental Section

Chemicals. Heptadecafluoro-1,1,2,2-tetrahydrodecyl trichlorosilane (CAS no. 78560-44-8) (F8H2) and *n*-octadecyl trichlorosilane (CAS no. 112-04-9) (H18) were supplied by Gelest, Inc., and used as received. All solvents (Aldrich) were of HPLC grade and used as received. The CO_2 (supplied by Air Products) was 99.9999% pure SCF/SFE grade carbon dioxide. The probing liquids for contact angle measurements were deionized (DI) water (resistivity > 16 M Ω cm) and diiodomethane (Aldrich, used as received).

Substrate Preparation. Single-side polished, 300 μm thick silicon wafers with [100] orientation (Virginia Semiconductor, Inc.) were cut into small pieces ($\approx 1 \times 1 \text{ cm}^2$) and placed into an ultraviolet/ozone (UVO) cleaner (Jelight Co., model 42, Suprasil lamp). They were exposed to the UVO treatment for 30 min. The UVO cleaner operates a low-pressure quartz–mercury lamp with UV radiation peaks at 184 and 254 nm. The radiation at 184 nm uses atmospheric molecular oxygen to produce ozone, which gets subsequently converted into (mono- and di-) atomic oxygen by irradiation with the 254 nm UV radiation. Atomic oxygen is a radical species that reacts with any hydrocarbon impurity at the sample surface, producing gaseous CO and CO_2 . In addition, atomic oxygen produces a silica surface with a high concentration of the surface –OH groups¹³ that serve as attachment points for the chlorosilane molecules at the silica surfaces.

General Notes on SAM Preparation from Chlorosilanes. The SAMs formed from trichlorosilane molecules that were used in this study follow the general reaction scheme shown in Scheme 1.² When a trace amount of water is present in the system, the $-\text{SiCl}_3$ gets hydrolyzed forming $-\text{Si(OH)}_3$ species. These react with the hydroxyl groups $\text{HO-[Si]}_{\text{substrate}}$ on the substrate.

SAM Preparation from Vapor. The SAM vapor deposition experiments were done in a desiccator that was connected to a mechanical vacuum pump. The vacuum level in the deposition chamber was kept at $\approx 10^{-2}$ to 10^{-3} Torr, so that there was still a sufficient amount of water molecules present for the reaction

given in Scheme 1. The sample was placed upside-down above the diffusion source, which consisted of a mixture of the chlorosilane and paraffin oil. Because the paraffin oil does not mix with the chlorosilane molecules, it provides a convenient diluent medium for the diffusion source; the flux of the chlorosilane molecules can be conveniently adjusted by simply varying the chlorosilane/paraffin oil ratio. All experiments were done at a chlorosilane/paraffin oil ratio of 1:1 (w/w). The vapor pressure for F8H2 is sufficiently high at room temperature, so the chlorosilane evaporates readily. However, the vapor pressure of H18 is relatively low at room temperature, so the H18/paraffin oil mixture was heated to 80 $^\circ\text{C}$ to increase the flux of H18 during the vapor deposition. The samples were exposed to the diffusing source for different time intervals ranging from seconds to hours. After the evaporation, the samples were immersed in and washed with warm (≈ 65 $^\circ\text{C}$) deionized water to remove any physisorbed molecules and subsequently dried with nitrogen.

SAM Preparation from Organic Solvent. The F8H2 molecules were dissolved in 1,1,2-trichloro trifluoroethane (concentration ≈ 35 mmol), and the H18 molecules were dissolved in toluene (concentration ≈ 5 mmol). The SAM deposition was carried out at room temperature by immersing the UVO-treated silicon wafers in the organic solvent SAM solutions for controlled time periods. After the SAM deposition, the samples were washed thoroughly with pure fluorinated solvent and immersed in and washed with warm (≈ 65 $^\circ\text{C}$) deionized water to remove any physisorbed molecules. Subsequently, the specimens were dried with nitrogen.

SAM Preparation from Liquid CO_2 . The deposition method consisted of four technological steps. First, the chlorosilane was mixed with CO_2 (concentration ≈ 28 mmol) at $P = 1000$ psi and $T = 297$ K in a mixing vessel for 24 h to ensure complete miscibility. In the second step, a fresh UVO-cleaned silicon wafer was placed in a coating chamber, which was subsequently pressurized without purging. In our experiments, the chamber was originally full of air at natural room humidity (normally between 40 and 50%, as measured using a PUL Thermo Hydrometer). The humidity provided moisture for the chemical reaction scheme to take place. The pressurization was terminated when the first traces of CO_2 condensation were detected. In the next step, the gas side of the apparatus was connected with the main coating chamber and the liquid CO_2 /silane solution was pumped from the mixing vessel into the coating chamber using a high-pressure gear pump. The solution was allowed to wet each substrate for a specified deposition time (i.e., 0 s, 10 s, etc.) so that the monolayer formation kinetics could be studied. Finally, the mixture was drained back to the mixing vessel at about 2 mm/s. The coating chamber was isolated and then purged with pure liquid CO_2 at saturation for 2–10 s to remove any physically adsorbed chlorosilane molecules. This purging process was repeated three times before the chamber was depressurized to atmospheric conditions. The deposition times, τ , are provided in the text. The case $\tau = 0$ s denotes a situation in which the wafer was contacted (< 2 s) with the chlorosilane solution in l-CO_2 and then immediately drained.

Experimental Techniques. Contact angle experiments were performed using a Ramé-Hart contact angle goniometer (model 100-00) equipped with a CCD camera and analyzed with the Ramé-Hart software. The advancing contact angles were read by injecting 6 μL of probing liquid; the receding contact angles were determined by removing 3 μL of probing liquid from the droplet. Each data point reported in the paper represents an average over five measurements on the same sample. The data points have an error better than $\pm 1.5^\circ$. By a combination of contact angle measurements using very polar (DI water) and very nonpolar (diiodomethane) liquids, a picture of the molecular organization within the SAM can be obtained. While the polar liquid is sensitive to the chain alignment within the SAM, the nonpolar liquid probes mainly the “in-plane” structure of the SAM.²

We examined the chemistry (including bond densities) and molecular orientation of the chlorosilane molecules on the SAM surfaces using NEXAFS.¹⁴ The NEXAFS experiments were carried out at the NIST/Dow Soft X-ray Materials Characterization Facility at the National Synchrotron Light Source at Brookhaven National Laboratory (NSLS BNL).¹⁵ NEXAFS

(13) Efimenko, K.; Genzer, J. Unpublished results.

involves the resonant soft X-ray excitation of a K or L shell electron to an unoccupied low-lying antibonding molecular orbital of σ symmetry, σ^* , or π symmetry, π^* .¹⁶ The initial state K shell excitation gives NEXAFS its element specificity, while the final-state unoccupied molecular orbitals provide NEXAFS with its bonding or chemical selectivity. A measurement of the partial electron yield (PEY) intensity of NEXAFS spectral features thus allows for the identification of chemical bonds and determination of their relative population density within the sample. Moreover, by collecting the PEY NEXAFS spectra at several θ ($20^\circ \leq \theta \leq 90^\circ$), where θ is the angle between the sample normal and the polarization vector of the X-ray beam, one can determine the surface molecular orientation of the SAM molecules on the silicon oxide surfaces. We express our results on the orientation of the molecules in the SAM in terms of the *average* tilt angle of either the fluorocarbon part of the single SF groups or the $-(\text{CH}_2)_{18}$ -zigzag. We note that the tilt angle determined from NEXAFS represents an *average* value. There is no straightforward way to discriminate between the case of all chains homogeneously tilted by the same angle and the case of a disordered system with a broad distribution of tilt angles. An important issue concerning the study of organic materials is the possibility of sample damage during the characterization with UV light, X-ray, and electron radiation. Semifluorinated materials are particularly sensitive to these effects.¹⁷ Hence, a fresh area of the sample was exposed to the X-ray beam spot for each measurement to minimize possible beam damage effects. Moreover, NEXAFS spectra showed no damage effects for at least three consecutive runs taken from the same spot on the sample. Moreover, due to the nature of the polarization dependencies of the NEXAFS signal intensities one cannot distinguish between a completely disoriented sample and a sample whose chains are all tilted by 54.7° , the so-called "magic angle".¹⁶

The SAM thickness was measured using a fixed geometry, fixed wavelength ($\lambda = 638$ nm) ellipsometer (Rudolph Technologies, model AutoEL II). The thickness of the SAM was evaluated from the measured ellipsometric angles Δ and ψ using the two-layer model in the DAF-IBM software. Following previous work, we assumed that the monolayer had an index of refraction equal to 1.45.²

Results

Semifluorinated SAMs. The upper panels in Figure 1 show contact angle data of deionized water (closed circles) and diiodomethane (open circles) collected from $\text{F}(\text{CF}_2)_8(\text{CH}_2)_2\text{SiCl}_3$ (F8H2) SAMs prepared by deposition from (a) vapor phase, (b) fluorinated solvent, and (c) l-CO_2 . The lower panels in Figure 1 depict the contact angle hysteresis (the difference between the advancing and receding contact angles) on the same materials. The data in Figure 1 show that regardless of the deposition medium, the contact angle increases with increasing deposition time and approaches a value of $\approx 113.7^\circ \pm 0.5^\circ$ for DI water and $\approx 96.5^\circ \pm 0.5^\circ$ for diiodomethane. However, the rate at which this saturation is reached depends crucially on the deposition technique. Specifically, the saturation value is reached after ≈ 200 min for the vapor deposition, > 500 min for the fluorinated solvent deposition, and only 20 s for the l-CO_2 medium. These data thus clearly illustrate that the SAM preparation from l-CO_2 is almost 600 times faster than

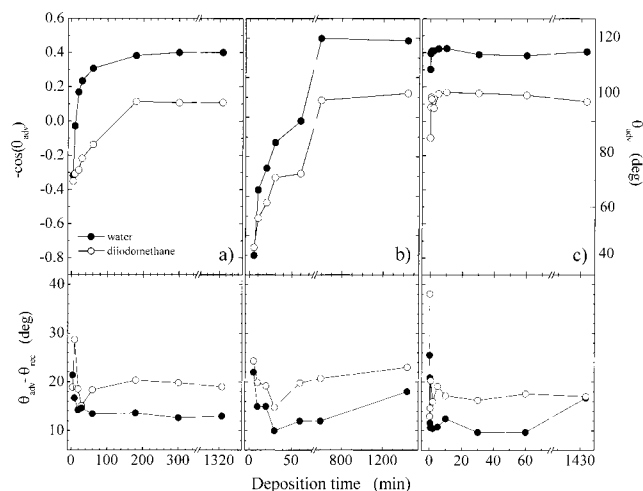


Figure 1. The upper panels show the cosine of the contact angle of deionized water (closed circles) and diiodomethane (open circles) on self-assembled monolayers made by depositing $\text{F}(\text{CF}_2)_8(\text{CH}_2)_2\text{SiCl}_3$ from vapor phase (a), fluorinated solvent (b), and liquid CO_2 (c). The lower panels depict the contact angle hysteresis (=the difference between the advancing and receding contact angles) on the same materials. The data have an average error of $\pm 1.5^\circ$.

that from the vapor phase and more than 1500 times faster than the classical solvent-based processes. Cao and co-workers also reported that l-CO_2 -based growth of SAMs is much faster than vapor or organic solvent depositions, but their kinetics are still slower than those observed by us.

A good estimate of the SAM uniformity can be obtained by monitoring the difference between the advancing and the receding contact angles. This difference, called the contact angle hysteresis, is a measure of the physical and chemical nonuniformity of the surface. The contact angle hysteresis for the SAMs prepared by the three deposition methods is shown in the lower panels of Figure 1. Figure 1a shows that the contact angle hysteresis decreases slightly with increasing deposition time at early times but levels off fairly rapidly and attains a value of $\approx 13^\circ$ for DI water and $\approx 20^\circ$ for diiodomethane. Interestingly, there seems to be a momentary increase in hysteresis at 10 min deposition. We attribute this to local rearrangement of the SAM chains at the silicon interface. The lower part of Figure 1b shows the hysteresis behavior of the SAMs deposited from the fluorinated solvent. Similar to the case of vapor deposition, the hysteresis initially decreases with increasing deposition time. However, after reaching a minimum it then starts to increase and reaches a value that is almost twice as high as that observed with the vapor-deposited specimen. This indicates that the growth of F8H2 SAMs from fluorinated solvents produces molecular arrays that are less perfect when compared to those grown via vapor deposition. The contact angle hysteresis measured on F8H2 SAMs deposited from l-CO_2 is shown in the bottom part of Figure 1c. Similar to the previous two cases, the hysteresis of water decreases with increasing time, reaches a minimum of $\approx 10^\circ$, but increases to $\approx 17^\circ$ for long deposition times. The behavior of the contact angle hysteresis of diiodomethane on the l-CO_2 -deposited F8H2 SAM shows a very interesting trend. At very short deposition times (15–30 s), the hysteresis reaches a minimum of $\approx 14^\circ$, subsequently increases to $\approx 19^\circ$, and for long deposition times reaches $\approx 17^\circ$. To understand the organization of the F8H2 molecules in the F8H2 SAMs

(14) See for example: Zharnikov, M.; Frey, S.; Rong, H.; Yang, Y. J.; Heister, K.; Buck, M.; Grunze, M. *Phys. Chem. Chem. Phys.* **2000**, *2*, 3359. Frey, S.; Heister, K.; Zharnikov, M.; Grunze, M.; Tamada, K.; Colorado, R.; Graupe, M.; Shmakova, E.; Lee, T. R. *Isr. J. Chem.* **2000**, *40*, 81. Bagus, P. S.; Weiss, K.; Schertel, A.; Wöll, C.; Braun, W.; Hellwig, C.; Jung, C. *Chem. Phys. Lett.* **1996**, *248*, 129.

(15) For the description of the NSLS BNL soft X-ray materials characterization facility, see: Fischer, D. A., et al. *Appl. Surf. Sci.* **1998**, *133*, 58.

(16) Stöhr, J. *NEXAFS Spectroscopy*; Springer-Verlag: Berlin, 1992.

(17) Jäger, B.; Schürmann, H.; Müller, H. U.; Himmel, H.-J.; Neumann, M.; Grunze, M.; Wöll, C. *Z. Phys. Chem.* **1997**, *202*, 263. Wirde, M.; Gelius, U.; Dunbar, T.; Allara, D. L. *Nucl. Instrum. Methods Phys. Res., Sect. B* **1997**, *131*, 245. Zharnikov, M.; Geyer, W.; Götzhäuser, A.; Frey, S.; Grunze, M. *Phys. Chem. Chem. Phys.* **1999**, *1*, 3163.

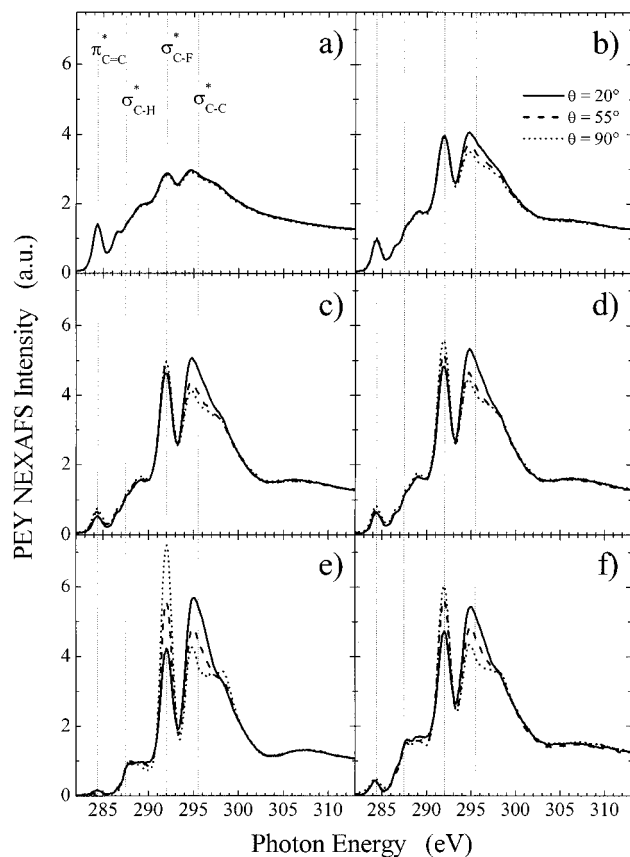


Figure 2. Partial electron yield NEXAFS intensity from self-assembled monolayers made by depositing $\text{F}(\text{CF}_2)_8(\text{CH}_2)_2\text{SiCl}_3$ from liquid CO_2 . The NEXAFS data were collected at $\theta = 20^\circ$ (solid lines), $\theta = 55^\circ$ (dashed lines), and $\theta = 90^\circ$ (dotted lines), where θ denotes the angle between the sample normal and the direction of the electric vector of the X-ray beam. The deposition times for the $\text{F}(\text{CF}_2)_8(\text{CH}_2)_2\text{SiCl}_3$ SAMs were 0 s (a) (see text for details), 10 s (b), 45 s (c), 2 min (d), 30 min (e), and 24 h (f). The vertical dashed lines denote the position of the NEXAFS transitions of the C=C bond ($1s \rightarrow \pi^*_{\text{C=C}}$, at 284.4 eV), the C-H bond ($1s \rightarrow \sigma^*_{\text{C-H}}$, at 287.5 eV), the C-F bond ($1s \rightarrow \sigma^*_{\text{C-F}}$, at 292.0 eV), and the C-C bond ($1s \rightarrow \pi^*_{\text{C-C}}$, at 295.0 eV).

grown from l-CO_2 , we performed time-dependent NEXAFS measurements to determine chain orientation at the silica surfaces.

Figure 2 shows the NEXAFS spectra from the F8H2 SAMs deposited from l-CO_2 . The NEXAFS data were collected at $\theta = 20^\circ$ (solid lines), $\theta = 55^\circ$ (dashed lines), and $\theta = 90^\circ$ (dotted lines), where θ denotes the angle between the sample normal and the direction of the electric vector of the X-ray beam. The deposition times for the $\text{F}(\text{CF}_2)_8(\text{CH}_2)_2\text{SiCl}_3$ molecules were (a) 0 s (sample washed with the $\text{l-CO}_2/\text{F8H2}$ chlorosilane solution), (b) 10 s, (c) 45 s, (d) 2 min, (e) 30 min, and (f) 24 h. Several characteristic peaks can be identified in the PEY NEXAFS spectra of the F8H2 SAM that correspond to the $1s \rightarrow \pi^*$ transition of the C=C bond ($E = 284.4$ eV) and $1s \rightarrow \sigma^*$ transitions associated with the C-H ($E = 287.5$ eV), C-F ($E = 292.0$ eV), and C-C ($E = 295.5$ eV) bonds. These are depicted with the vertical dashed lines in Figure 2. By inspection of the NEXAFS data in Figure 2, the following picture emerges. When the sample is briefly exposed to the $\text{l-CO}_2/\text{F8H2}$ chlorosilane solution (ca. 2 s), several F8H2 chlorosilane molecules get attached to the substrate but they are not oriented. As the deposition time increases, more molecules get attached to the substrate and they also seem to orient. The latter conclusion is based on the observation that the intensities originating from the $1s \rightarrow \sigma^*_{\text{C-F}}$ and

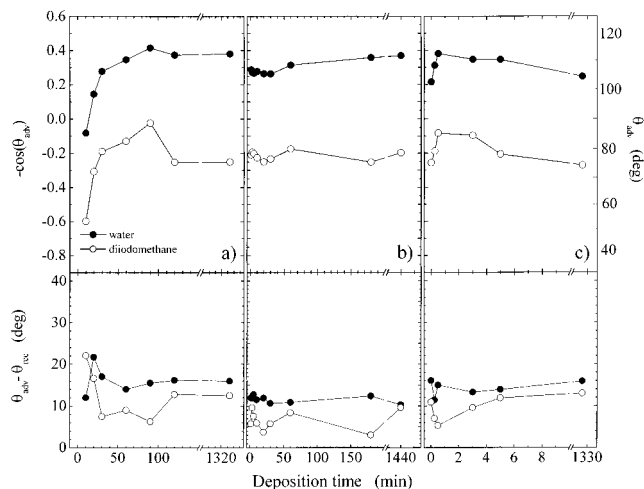


Figure 3. The upper panels show the cosine of the contact angle of deionized water (closed circles) and diiodomethane (open circles) on self-assembled monolayers made by depositing $\text{H}(\text{CH}_2)_{18}\text{SiCl}_3$ from vapor phase (a), toluene (b), and liquid CO_2 (c). The lower panels depict the contact angle hysteresis (=the difference between the advancing and receding contact angles) on the same materials. The data have an average error of $\pm 1.5^\circ$.

$1s \rightarrow \sigma^*_{\text{C-C}}$ transitions change with varying angle θ ; as θ increases, the intensity corresponding to σ^* of the C-F bond increases while that of the C-C bond decreases. The orientation of the F8H2 SAM molecules on the silica substrate can be inferred by qualitatively examining the PEY NEXAFS data. The $\sigma^*_{\text{C-F}}$ signal in the NEXAFS spectra collected at $\theta = 90^\circ$ is always stronger than that measured at $\theta = 20^\circ$; thus the director of the F8H2 SAM molecules is only slightly tilted away from the sample normal. Careful inspection of the time-dependent NEXAFS spectra in Figure 2 reveals that the intensity of the $\sigma^*_{\text{C-F}}$ signal increases with increasing time, reaches a maximum for 30 min (cf. Figure 2e), and then decreases slightly for long deposition times. This behavior is an indication of the “perfection” of the molecular orientation of the F8H2 moieties in the SAM for $\tau < 30$ min followed by chain reorganization at longer deposition times. A more detailed analysis presented recently^{18,19} can be used to elucidate the average angular orientation of the fluorocarbon helix within the F8H2 SAM. The results are discussed later in the paper.

Hydrocarbon SAMs. The upper panels in Figure 3 show contact angle data of deionized water (closed circles) and diiodomethane (open circles) collected from $\text{H}(\text{CH}_2)_{18}\text{SiCl}_3$ (H18) SAMs prepared by deposition from (a) vapor phase, (b) toluene, and (c) l-CO_2 . The lower panels in Figure 3 depict the contact angle hysteresis (the difference between the advancing and receding contact angles) on the same materials. Similar to the behavior observed in the F8H2 SAM, the data in Figure 3 indicate that the contact angle increases with increasing deposition time in all cases. There is some difference in the final stages of the deposition process, however. While the contact angles of DI water and diiodomethane on H18 SAMs deposited from vapor and toluene saturate at $\approx 112.0^\circ \pm 0.5^\circ$ and $\approx 78.0^\circ \pm 1.0^\circ$, respectively, the corresponding

(18) Genzer, J.; Sivaniah, E.; Kramer, E. J.; Wang, J.; Körner, H.; Xiang, M.; Char, K.; Ober, C. K.; DeKoven, B. M.; Bubeck, R. A.; Chaudhury, M. K.; Sambasivan, S.; Fischer, D. A. *Macromolecules* **2000**, *33*, 1882.

(19) Genzer, J.; Sivaniah, E.; Kramer, E. J.; Wang, J.; Körner, H.; Char, K.; Ober, C. K.; DeKoven, B. M.; Bubeck, R. A.; Fischer, D. A.; Sambasivan, S. *Langmuir* **2000**, *16*, 1993.

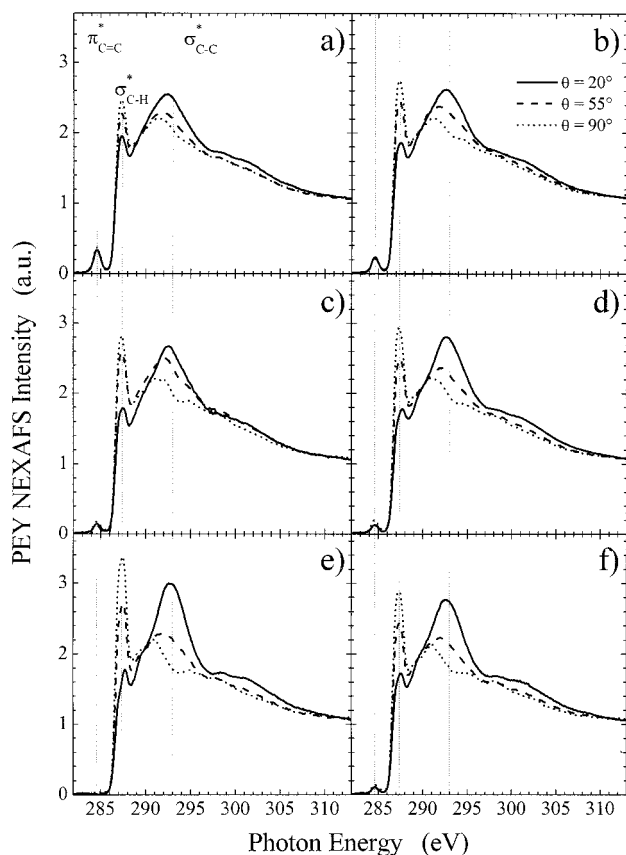


Figure 4. Partial electron yield NEXAFS intensity from self-assembled monolayers made by depositing $\text{H}(\text{CH}_2)_{18}\text{SiCl}_3$ from liquid CO_2 . The NEXAFS data were collected at $\theta = 20^\circ$ (solid lines), $\theta = 55^\circ$ (dashed lines), and $\theta = 90^\circ$ (dotted lines), where θ denotes the angle between the sample normal and the direction of the electric vector of the X-ray beam. The deposition times for the $\text{H}(\text{CH}_2)_{18}\text{SiCl}_3$ SAMs were 0 s (a) (see text for details), 15 s (b), 30 s (c), 3 min (d), 5 min (e), and 22 h (f). The vertical dashed lines denote the position of the NEXAFS transitions of the C=C bond ($1s \rightarrow \pi^*_{\text{C=C}}$, at 284.4 eV), the C-H bond ($1s \rightarrow \sigma^*_{\text{C-H}}$, at 287.5 eV), and the C-C bond ($1s \rightarrow \pi^*_{\text{C-C}}$, at 293.0 eV).

values measured on the H18 SAM deposited from $l\text{-CO}_2$ are slightly lower ($\approx 105.0^\circ \pm 1.5^\circ$ and $\approx 74.0^\circ \pm 1.0^\circ$).

NEXAFS was used to measure the chain orientation in the H18 SAM samples. Figure 4 shows the NEXAFS spectra from the H18 SAMs deposited from $l\text{-CO}_2$. The NEXAFS data were collected at $\theta = 20^\circ$ (solid lines), $\theta = 55^\circ$ (dashed lines), and $\theta = 90^\circ$ (dotted lines). The deposition times for the $\text{H}(\text{CH}_2)_{18}\text{SiCl}_3$ molecules were (a) 0 s (sample washed with the $l\text{-CO}_2/\text{F8H2}$ chlorosilane solution), (b) 15 s, (c) 30 s, (d) 3 min, (e) 5 min, and (f) 22 h. The various peaks in the PEY NEXAFS spectra of the H18 SAM, whose positions are indicated by the vertical lines, correspond to the $1s \rightarrow \pi^*$ transition of the C=C bond ($E = 284.4$ eV) and $1s \rightarrow \sigma^*$ transitions associated with the C-H ($E = 287.5$ eV) and C-C ($E = 293.0$ eV) bonds. Because the $1s \rightarrow \sigma^*_{\text{C-H}}$ and $1s \rightarrow \sigma^*_{\text{C-C}}$ transition intensities change with varying θ (as θ increases, the intensity of the corresponding $\sigma^*_{\text{C-H}}$ increases while that of $\sigma^*_{\text{C-C}}$ decreases), one can conclude that the chains in the H18 SAM are oriented. Similar to the case of the F8H2 SAMs on the silica substrate, the orientation in the H18 SAM can be deduced by qualitatively examining the PEY NEXAFS data of the H18 SAM. The $\sigma^*_{\text{C-H}}$ signal in the NEXAFS spectra collected at $\theta = 90^\circ$ is always stronger than that measured at $\theta = 20^\circ$; thus the director of the H18 SAM molecules is only slightly tilted away from the

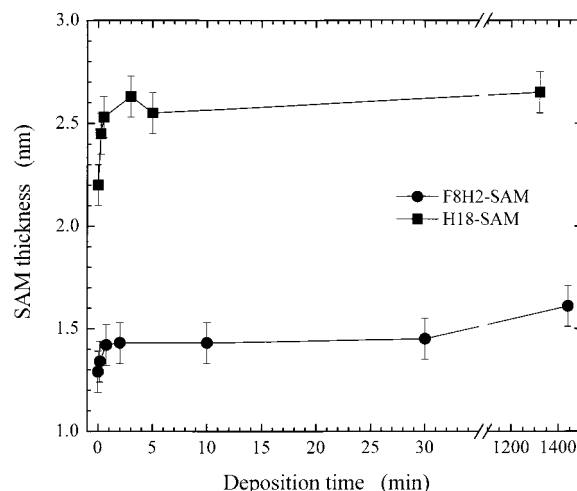


Figure 5. Ellipsometric thickness of the F8H2 SAM (circles) and the H18 SAM (squares) as a function of the deposition time from liquid CO_2 mixtures. The lines are guides to the eye.

sample normal. By comparing the NEXAFS spectra in Figure 4, one sees that when exposed for a short time to the H18/ $l\text{-CO}_2$ solution, the H18 molecules chemically bond to the substrate and adopt some orientational order. Recall that this is in contrast to the behavior detected in the F8H2 SAMs where the molecules initially adsorb with no orientation. The spectra in Figure 4 show that with increasing deposition time, the difference between the intensities of the $\sigma^*_{\text{C-H}}$ and $\sigma^*_{\text{C-C}}$ signals increases, reaches a maximum for 5 min (cf. Figure 4e), and then decreases slightly for long deposition times. Hence, similar to the behavior detected in the F8H2 SAM, the H18 chains in the H18 SAM reorganize at longer deposition times. A more detailed analysis presented elsewhere¹⁶⁻¹⁹ can be used to evaluate the average angular orientation of the hydrocarbon chains in the H18 SAM.

Discussion

By combining the contact angle, ellipsometry, and NEXAFS data, one can reconstruct the steps involved in the adsorption and growth of the SAMs. Our contact angle and ellipsometry data (cf. Figure 5) reveal that initially, the adsorption takes place very rapidly. Within the first several minutes, most of the substrate gets covered by the SAM. This rapid adsorption regime (several seconds to minutes) is followed by a slower adsorption kinetics regime (on the order of minutes to hours), during which the remaining free sites on the surface are filled by the SAM molecules. Hence, in accord with previous studies,^{9,10} we presuppose that the mass transfer from the bulk to the substrate takes place in two steps.

Many authors studied the formation of SAMs (mainly thiols on gold). Several experimental probes were utilized, including ellipsometry,²⁰ second harmonic generation,²¹ infrared (IR) spectroscopies,^{10,22} and quartz crystal microbalance,²³ to evaluate the time dependence of the fractional coverage of the SAM on the substrate, $\phi(\theta)$. Several authors used multiple techniques in their kinetic studies; they pointed out that SAMs might have different structural properties and anisotropies and there is not a

(20) Bain, C. D.; Troughton, E. B.; Tao, Y.; Evall, J.; Whitesides, G. M.; Nuzzo, R. G. *J. Am. Chem. Soc.* **1989**, *111*, 321.

(21) Buck, M.; Eisert, F.; Fischer, J.; Grunze, M.; Täger, F. *Appl. Phys. A* **1991**, *53*, 552. Dannenberger, O.; Buck, N.; Grunze, M. *J. Phys. Chem. B* **1999**, *103*, 2202.

(22) Chen, S. H.; Frank, C. F. *Langmuir* **1989**, *5*, 987.

(23) Kim, Y.; McCarley, R. L.; Bard, A. J. *Langmuir* **1993**, *9*, 1941.

Table 1. Diffusivity, Silane Concentration, and Adsorption Rate Constant Estimates for F8H2 SAMs and H18 SAMs Deposited from Vapor, Liquid CO₂, and Toluene

deposition method	D (cm ² s ⁻¹)	F8H2 SAM			H18 SAM		
		C_b (mmol L ⁻¹)	k_{af} (L mmol ⁻¹ min ⁻¹)	k_{ar} (min ⁻¹)	C_b (mmol L ⁻¹)	k_{af} (L mmol ⁻¹ min ⁻¹)	k_{ar} (min ⁻¹)
vapor	$\approx 2.3 \times 10^2$	$\approx 5.4 \times 10^{-4}$	≈ 347	$\approx 7 \times 10^{-3}$	$\approx 4.5 \times 10^{-4}$	≈ 325	$\approx 3 \times 10^{-3}$
liquid CO ₂	$\approx 7.0 \times 10^{-5}$	≈ 28	≈ 12	$\approx 5 \times 10^{-2}$	≈ 35	≈ 8	$\approx 5 \times 10^{-1}$
organic solvent ^a	$\approx 6.0 \times 10^{-6}$	≈ 35	$\approx 2 \times 10^{-3}$	$\approx 6 \times 10^{-3}$	≈ 44	$\approx 2 \times 10^{-1}$	$\approx 3 \times 10^{-1}$

^a The organic solvents were 1,1,2-trichloro trifluoroethane (F8H2 SAM) and toluene (H18 SAM).

single technique that would provide completely unambiguous information about the structure and coverage of the SAMs.^{22,24} These authors demonstrated that the time dependence of contact angles mirrors that of IR and ellipsometry signals.^{22,24} In this work, the time dependence of the contact angle will be used to evaluate $\phi(t)$ and the data can be fitted to the adsorption and diffusion-limited models providing estimates of the rate constants for the forward and reversible adsorption process, k_{af} and k_{ar} , respectively. Values of k_{af} and k_{ar} could *only be estimated* from the contact angle data because θ_{measured} can be dependent on the molecular arrangement of species and the packing density. We point out that our ellipsometry data help to corroborate the kinetic results and the existence of the monolayer.

An estimate of the surface coverage can be elucidated from the contact angle data using the Israelachvili–Gee equation,²⁵ which relates the contact angle of a heterogeneous surface, θ_{mix} , composed of two chemically different species (1, 2) to the contact angle of the pure species (θ_1 , θ_2) and the area fraction of each species in the mixture (ϕ_1 , ϕ_2):

$$[1 + \cos(\theta_{\text{mix}})]^2 = \phi_1 [1 + \cos(\theta_1)]^2 + \phi_2 [1 + \cos(\theta_2)]^2 \quad (1)$$

Realizing that $\phi_1 + \phi_2 = 1$, eq 1 can be rearranged to give an expression for the time-dependent surface coverage of one of the species in the heterogeneous surface:

$$\phi_1 = \frac{[1 + \cos(\theta_{\text{mix}})]^2 - [1 + \cos(\theta_2)]^2}{[1 + \cos(\theta_1)]^2 - [1 + \cos(\theta_2)]^2} \quad (2)$$

An expression relating an estimate of the surface coverage of the monolayer on the silica substrate to the experimentally measured contact angle ($\theta_{\text{measured}}(t)$) can be written using eq 2; the heterogeneous surface is composed of a mixture of units of either pure monolayer ($\theta_{\text{SAM},\infty}$) or surface hydroxyl groups ($\cos(\theta_{\text{OH}}) \approx 1$):

$$\phi_{\theta_{\text{SAM},\infty}}(t) = \frac{[1 + \cos(\theta_{\text{measured}}(t))]^2 - 4}{[1 + \cos(\theta_{\text{SAM},\infty})]^2 - 4} \quad (3)$$

To obtain the area fraction covered with pure monolayer, ($\phi_{\theta_{\text{SAM},\infty}}(t)$), from the time-dependent $\theta_{\text{measured}}(t)$ values, we use the established values of $\theta_{\text{SAM},\infty} = 113.5^\circ$ and 112.0° for monolayers composed of pure F8H2 and pure H18, respectively.

Our attempts to fit the experimental data to the diffusion-limited model failed. The functional form given by eq 15 in Appendix A does not reproduce the experimental data. Specifically, eq 15 is not capable of capturing the saturation of the SAM coverage at higher deposition times. In contrast, the adsorption-limited model was capable of fitting the experimental data well. It is therefore

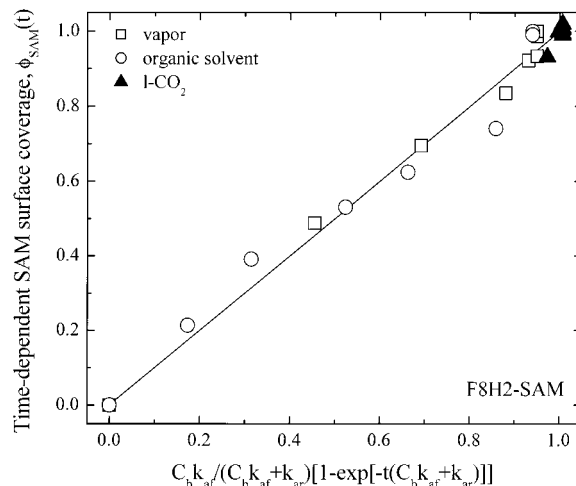


Figure 6. Coverage of the F8H2 SAM on a silicon oxide surface as a function of the adsorption time for the deposition from vapor (open circles), organic solvent (open squares), and liquid CO₂ (closed up-triangles) evaluated using the adsorption-limited model described in the text.

the adsorption of the molecule to the surface and not the diffusion from the bulk that is the primary mechanism controlling the SAM formation rate. We have fitted the experimental data to eq 10 and used eqs 11 (see Appendix A) to evaluate k_{af} and k_{ar} . The values of k_{af} and k_{ar} obtained from the fits are reported in Table 1 for both the F8H2 SAM and the H18 SAM. Figure 6 shows the time-dependent coverage $\phi(t)$ for F8H2 SAMs deposited from vapor (open circles), organic solvent (open squares), and liquid CO₂ (closed up-triangles) evaluated using the adsorption-limited model. The abscissa in the plot was chosen such that the data give a straight line with the slope of 1.

Even though k_{af} and k_{ar} are *only estimates*, there are still important conclusions that can be drawn from the data. Table 1 reveals that k_{af} for the vapor phase is 2–3 orders of magnitude higher than that of k_{af} in l-CO₂. Similarly, k_{af} in the vapor phase is 4–6 orders of magnitude higher than k_{af} in the organic solvent. Hence, on the basis of the rate constants the rate of adsorption follows the following trend: vapor phase > l-CO₂ > organic solvent. However, the observed rate of reaction is fastest in l-CO₂. The dramatic rise in the adsorption rate in l-CO₂, relative to vapor-phase deposition (cf. Figures 1 and 3, parts a and c), is a result of the much higher chlorosilane concentration ($\approx 50\,000$ times greater in l-CO₂). The differences between the kinetic parameters for vapor, organic, and l-CO₂ deposition could be due to a number of possibilities, including changes in the ability of the molecule to orient with a reactive site on the surface, different reaction mechanisms with the surface, and so forth. Some of these distinctions also become evident when one compares the different values of k_{ar} . Adsorption from the vapor phase is almost completely irreversible, $K_{\text{eq}} (=k_{af}/k_{ar}) \gg 1$, because k_{ar} is 4–5 orders of magnitude smaller than k_{af} . However, the same conclusion does not hold for adsorption from

(24) Shon, Y.-S.; Lee, T. R. *J. Phys. Chem. B* **2000**, *104*, 8182.

(25) Israelachvili, J. N.; Gee, M. L. *Langmuir* **1989**, *5*, 288.

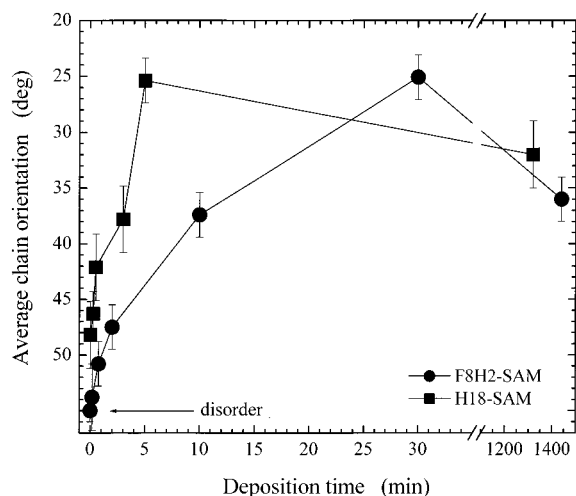


Figure 7. Average tilt of the molecules in the F8H2 SAM (circles) and the H18 SAM (squares) as a function of the deposition time from liquid CO_2 mixtures. The average tilt was determined from the NEXAFS measurements, as detailed in the text. The lines are guides to the eye.

either organic solvent or l-CO_2 . For the organic solvent, $K_{\text{eq}} < 1$ for both the fluorinated and nonfluorinated molecules. This means that the silane molecules will not remain on the surface for long periods of time but will instead quickly desorb. Only those molecules arriving to the substrate that are close to the optimal reaction orientation will be able to create a permanent bond with the surface. In l-CO_2 , the situation is different. $K_{\text{eq}} > 1$ for both the fluorinated and hydrocarbon species. Therefore, most of the molecules will adsorb to the surface while only a few will desorb. Could this be the reason that SAMs form faster in l-CO_2 ? Unlike in organic solvents, the molecules in l-CO_2 would not have to approach the surface in the optimal orientation to react but could instead reorient on or near the surface. Other explanations for the faster reaction rate include (i) a change in reaction mechanism or (ii) possible differences in the way water (a key reaction component) interacts with the surface in the two solvent environments. Clearly, more work needs to be undertaken to determine the actual mechanisms.

Our final remark concerns orientational aspects of the SAM that occur during the monolayer formation. Previously, we discussed that the molecular transport from the bulk to the substrate follows two regimes. These are very similar to those for both the hydrocarbon and the semifluorinated molecules. Our NEXAFS analysis reveals that there is yet another regime in the SAM-forming process, associated with the organization of the molecules within the SAM, in which the H18 and F8H2 SAMs follow different organization kinetics. We mentioned that in the initial adsorption step, very rapid adsorption of the chlorosilanes occurs on the silica surface within the first ≈ 1 s. Ellipsometry measurements reveal (cf. Figure 5) that neither the F8H2 SAM nor the H18 SAM monolayer is complete. Interestingly, while the adsorbed F8H2 molecules are not oriented, there seems to be an orientation within the H18 SAM monolayer. A more detailed analysis reveals that the average chain tilt, $\langle \tau \rangle$, is $\approx 48^\circ$ (cf. Figure 7). We attribute this behavior to higher solubility of the F8H2 molecules in CO_2 (as compared to their hydrocarbon counterparts). Thus, while the F8H2 moieties prefer to be surrounded by the CO_2 solvent, the phase separation between hydrocarbon and CO_2 leads to close packing in the H18 SAM. In the second step of the deposition process, more molecules are added to the substrate and the

monolayer growth is complete at ≈ 3 and ≈ 1 min for the F8H2 SAM and the H18 SAM, respectively. During this second step of the deposition process, the chains orient such that the main helical axis of both the rigid fluorocarbon part of F8H2 and the planar zigzag $-(\text{CH}_2)_{18}-$ helix of H18 tilts more toward the sample normal. The reorientation kinetics is faster in the H18 SAM case. The chemical incompatibility between the hydrocarbon molecules and CO_2 is presumably responsible for the faster deposition process and hence faster chain rearrangement relative to that of the F8H2 SAM. Finally, after long deposition times (several hours), there seems to be slight "relaxation" of the initial structures indicated by a slight reorientation of the F8H2 helices and also in-plane rearrangement of the terminal $-\text{CF}_3$ groups (as indicated by the contact angle data). Similarly, the $-(\text{CH}_2)_{18}-$ helix in the H18 SAM seems to be tilting farther away from the sample normal at very long deposition times. Because the overall monolayer thickness does not change between short and long deposition times, we attribute the chain reorganization on the surface to a possible minute chain desorption followed by increased chain packing within the SAM. In fact, the $\langle \tau \rangle$ detected at very long deposition times ($\approx 36^\circ$ for the F8H2 SAM and $\approx 32^\circ$ for the H18 SAM) follows the molecular tilt quantization previously reported for the F8H2 SAM²⁶ and the H18 SAM.² Thus, our combined contact angle, ellipsometry, and NEXAFS analysis reveals several adsorption/organization steps involved in the formation of SAMs. Clearly, more work is needed to uncover detailed descriptions of each of the transport and assembling processes.

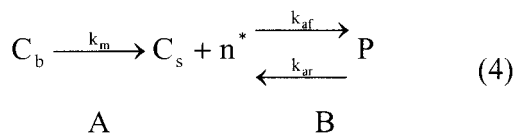
Summary. We studied the formation of semifluorinated and hydrocarbon self-assembled monolayers by deposition of their respective trichlorosilane precursors from vapor, organic solvent, and l-CO_2 . We used contact angle measurements and ellipsometry to follow the deposition kinetics of the molecules. Our results indicate that regardless of the type of the molecule, the deposition rates from l-CO_2 exceed the deposition kinetics from vapor or organic solvents by several orders of magnitude. We derive two different transport models describing the formation of SAMs. We show that while the diffusion-limited model is not capable of describing the experimental data, the adsorption-limited model captures the major features of the adsorption kinetics quite well. We apply the results of the adsorption-limited model to conclude that the observed behavior is a consequence of (i) a relatively high bulk concentration (l-CO_2 vs vapor) and (ii) higher solution diffusivity (l-CO_2 vs organic solvent) of the silanes in l-CO_2 . NEXAFS was used to monitor the orientation of the F8H2 and H18 molecules in their corresponding SAMs as a function of time. Our NEXAFS data reveal that for deposition from l-CO_2 , the F8H2 molecules adsorb initially without any molecular order in the monolayer. As more F8H2 molecules adsorb at the silicon oxide substrate, they start to organize and orient. A complete monolayer order is achieved after ≈ 30 min exposure to the l-CO_2 solution of F8H2. The molecular behavior of H18 moieties in the H18 SAMs was found to be different. Already after washing the silica substrate with a H18/ l-CO_2 solution, the H18 molecules adsorb and form an organized layer. Similar to the case of the semifluorinated species, the order in the H18 SAM increases with increasing time and approaches a constant value after ≈ 5 min exposure to the H18/ l-CO_2 solution. We attribute the difference in the orientation kinetics to the different solubilities of F8H2 and H18 in l-CO_2 . Specifically, while a higher solubility of the

fluorinated part of the F8H2 molecule in l-CO₂ slows down the complete monolayer organization, the high chemical incompatibility between the H18 moieties and l-CO₂ leads to rapid reorientation of the H18 SAMs on the substrate. In addition, we state that possible intermolecular interactions between neighboring F8H2 chains may also be responsible for the slower organization kinetics in the F8H2 SAM. In both the F8H2 SAM and the H18 SAM, we see that at longer deposition times (\approx hours), the molecules in the SAM start to tilt slightly away from the sample normal. We speculate that this behavior is a combination of several processes involving adsorption-desorption dynamics and local molecular rearrangement.

Acknowledgment. This research was supported through a grant from the Kenan Center for the Utilization of Carbon Dioxide in Manufacturing. Partial support from the NSF CAREER award, Grant No. DMR98-75256 (J.G.) and from the NSF STC award, Grant No. CHE-9876674 (B.N.) is also appreciated. The NEXAFS experiments were carried out at the National Synchrotron Light Source, Brookhaven National Laboratory, which is supported by the U.S. Department of Energy, Division of Materials Sciences and Division of Chemical Sciences. We thank Drs. Daniel Fischer and William Wallace (both at NIST) for their assistance during the course of the NEXAFS measurements.

Appendix A: Rate Models for SAM Adsorption

The rate of self-assembled monolayer formation is of particular interest since the monolayer forms at different rates in each of the three solvents. A kinetic model to describe this process can be developed by assuming that the surface reaction occurs at a high rate after adsorption of a chemical species to the reaction site. In this case, there are two significant events that must occur for the surface reaction to proceed: diffusion of the reactive species from the bulk solution to the surface and adsorption of the molecule onto a reactive surface site. The reaction mechanism can be written as



In eq 4, C_b is the bulk concentration of the reactant, C_s is the surface concentration of reactant, n^* is the concentration of free reactive sites, P is the adsorbed species prior to reaction, and k_{af} and k_{ar} are rate constants for the reversible adsorption process. The rate of diffusion (A, eq 4) and the rate of adsorption (B, eq 4) can be written as

$$R_A = k_m(C_b - C_s) \quad (5)$$

$$\begin{aligned} R_B = k_{af}C_s n^* - k_{ar}P &= k_{af}C_s N(1 - \phi) - k_{ar}N\phi = \\ & k_{af}N \left[C_s(1 - \phi) - \frac{\phi}{K_{eq}} \right] \end{aligned} \quad (6)$$

where ϕ is the fractional surface coverage, N is the total number of sites, and $K_{eq} = k_{af}/k_{ar}$.

Two different rate expressions can be derived for the monolayer formation if each of the significant processes (diffusion and adsorption) is treated as being rate limiting. When the adsorption process is considered to be rate limiting, then

$$\frac{R_A}{k_m} \approx 0 \quad \text{and} \quad C_s \approx C_b \quad (7)$$

Substituting the results of (7) into the limiting rate expression (6) gives

$$\frac{d\phi}{dt} = k_{af}C_b(1 - \phi) - k_{ar}\phi \quad (8)$$

and after integration, realizing now that θ varies with time, $\phi(t)$,

$$\phi(t) = \frac{C_b k_{af}}{C_b k_{af} + k_{ar}} - \frac{\exp[-(C_b k_{af} + k_{ar})t - (C_b k_{af} + k_{ar})C_{int}]}{C_b k_{af} + k_{ar}} \quad (9)$$

The integration constant C_{int} in eq 9 can be eliminated by considering the initial condition $\phi(t=0) = 0$ leading to

$$\phi(t) = \frac{\beta}{\alpha} [1 - \exp[-\alpha t]] \quad (10)$$

where

$$\alpha = C_b k_{af} + k_{ar} \quad (11a)$$

$$\beta = C_b k_{af} \quad (11b)$$

In contrast, if the diffusion process is considered to be rate limiting,

$$\frac{R_B}{k_{af}} \approx 0 \quad \text{and} \quad C_s \approx \frac{\phi}{K_{eq}(1 - \phi)} \quad (12)$$

Substituting the results of eq 12 into the limiting rate expression (5) gives

$$\frac{d\phi}{dt} = \frac{k_m}{N} \left[C_b - \frac{\phi}{K_{eq}(1 - \phi)} \right] \quad (13)$$

and after integration

$$t = \frac{N}{k_m} \frac{K_{eq}}{C_b K_{eq} + 1} \phi - \frac{N}{k_m} \frac{K_{eq}}{(C_b K_{eq} + 1)^2} \ln(\phi + C_b K_{eq} \phi - C_b K_{eq}) - C_{int} \quad (14)$$

Equation 14 can again be simplified by combining constants, considering the initial condition $\phi(t=0) = 0$, and expressing the time dependence of ϕ :

$$t = \frac{\alpha}{(\beta + 1)^2} [\beta\phi(t) + \phi(t) - \ln(1 - \phi(t) - \beta\phi(t))] \quad (15)$$

where

$$\alpha = \frac{N}{k_m} K_{eq} = \frac{N}{k_m} \frac{k_{af}}{k_{ar}} \quad (16a)$$

$$\beta = C_b K_{eq} = C_b \frac{k_{af}}{k_{ar}} \quad (16b)$$

Appendix B: Determining the Diffusivities of Chlorosilanes

An estimate of the diffusion coefficient for a species in low-density gaseous mixtures can be accomplished using

the derivation of Jeans, Chapman, and Sutherland.²⁷ The gas is considered to be either static or in the laminar regime and to be made of particles that possess equal size, mass, and velocity. Furthermore, the gas is assumed to be in the ideal state and the particles are assumed to be hard spheres:

$$D_{AA} = \frac{2}{3\pi^{3/2} d^2 P} \left(\frac{\kappa^3 T^3}{m} \right)^{1/2} \quad (17)$$

where D_{AA} is the mass diffusivity, P is the pressure, T is the temperature, κ is the Boltzmann constant, m is the mass of one molecule, and d is the diameter of one molecule (assumed to be spherical). For the F8H2 molecule, the mass of one particle is

$$m = \frac{M_w}{N_A} = \frac{528 \text{ g/mol}}{6.022 \times 10^{23} \text{ molecules/mol}} \quad (18)$$

where M_w is the molecule weight and N_A is Avogadro's number. The diameter of one particle can be estimated from the density:

(27) Welty, J. R.; Wicks, C. E.; Wilson, R. E. *Fundamentals of Momentum, Heat, and Mass Transfer*; John Wiley & Sons: New York, 1984.

$$d = 2 \left(\frac{3}{4\pi} V \right)^{1/3} = 2 \left(\frac{3}{4\pi} \frac{m}{\rho} \right)^{1/3} \quad (19)$$

where V is the volume of one particle and ρ is the bulk density. In our case, $\rho = 1.703 \text{ g/cm}^3$.

The diffusion coefficient of chlorosilane molecules in the liquid phase (carbon dioxide and fluorinated solvent) can be estimated since the solutions are dilute. In this case, the Stokes–Einstein equation applies:²⁸

$$D_{AB} = \frac{\kappa T}{6\pi r \mu_B} \quad (20)$$

where D_{AB} is the diffusivity of A in B, r is the radius of one particle, and μ_B is the solvent viscosity. The radius is $d/2$ shown above. The viscosities of carbon dioxide and 1,1,2-trichloro trifluoroethane are approximately 0.06 and 0.68 cP, respectively.²⁹

LA011813J

(28) Bird, R. B.; Stewart, W. E.; Lightfoot, E. N. *Transport Phenomena*; John Wiley & Sons: New York, 1960.

(29) Yaws, C. L. *Chemical Properties Handbook*; McGraw-Hill: New York, 1999.